12

Electromagnetic Sensor Technology for Biomedical Applications

Larissa V. Panina
School of Computing & Mathematics, University of Plymouth, United Kingdom

1. Introduction

Magnetic bio-detection constitutes a large area of research and development driven by its potential to provide versatile diagnostic tools in biology and medicine. Specific sensing technology is used depending on the applications which can be subdivided in two main groups: measuring a magnetic field from people and detecting magnetically labelled bio substances. The human body is mostly composed of what is normally regarded as nonmagnetic materials. In reality, every substance has some magnetic sensitivity, however small, being paramagnetic or diamagnetic. Their response is greatly limited by thermal fluctuations. In addition to this there is a further source of a magnetic field due to the neural activity which operates continuously throughout a living body. This neural activity involves movement of electric charges and, as such gives rise to magnetic fields. In principle, these fields represent a description of the neural activity and can be studied to help understanding the workings of the human body as well as provide an aid to diagnosis. On the other hand, they can be predicted and quantified by the fundamental laws of electromagnetic. In the other stream of applications, the use of magnetic labels allows the detection of various bio molecular reactions in immunoassays. It also results in a number of additional functionalities, such as transport of bio-molecules to a specific location, on-chip magnetic immuno-separation and testing or accelerating bio-molecular binding events.
The magnitudes of the magnetic fields involved are very small, being in the sub-nanoTesla region and their detection requires very sensitive instrumentation. We have extremely sensitive magnetic technology: SQUID magnetometer (superconducting quantum interference device). The noise level of the SQUID detection is in femto-Tesla so it could become an ideal instrument for studying magnetic fields from biological subjects (see, for example, Sternickel & Braginski, 2006). However, the cost involved and the complex cryogenic technology present huge hurdles that have prevented SQUID (including high transition temperature requiring liquid nitrogen) from becoming widely used. Several field measurements from various parts of the body were published and summarised in (Wikswo , 1999). Figure 1 presents comparison of some common magnetic fields and those generated by different parts of the human body. The signals from the brain are at about 1 picoTesla or less but from other parts of the body (such as the eyes and the stomach) are at levels an order of magnitude larger. One of the largest signals results from the heart which is at the level of about 25pT. The detection of this level of a magnetic field does not require all the

potential of SQUIDs and other high performance magnetometers (Ripka, 2001) can be used. Here we will discuss the potential of using as biosensors such magnetometers as giant magnetoresistive (GMR) and giant magnetoimpedance (GMI) sensors placing emphasis on a relatively new GMI sensing technology which could overcome many limitations of SQUID and magnetoresistive sensing platforms. As far as the detection of magnetic labels is concerned, we will consider the advantages of the detection method based on non linear magnetisation of magnetic labels through generation of high frequency harmonic spectra often referred to as magnetic particle spectral method (MPS). In both GMI and MPS the dynamic magnetisation processes are involved and we categorise them as electromagnetic bio sensing platform.

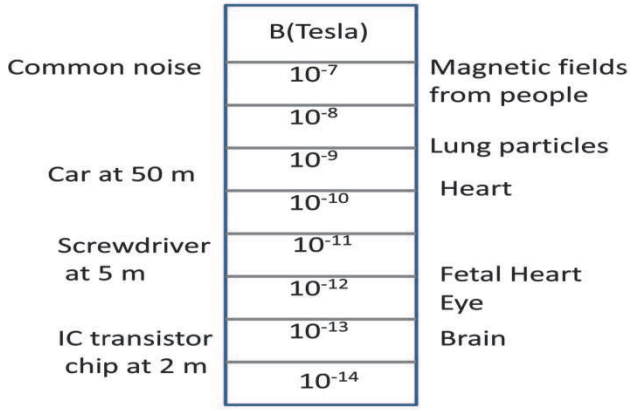

Fig. 1. Comparison of some common magnetic fields with those from human body.

Magnetoresitive sensing technology benefits from recent research and technological advances aiming the design of ultra high density magnetic memory hard discs and write/read heads (Prinz, 1998; Wolf 2001). However, limited sensitivity prevents the use of GMR sensors for measuring human magnetic fields, but they have been used to detect a variety of commercially available magnetic micro and nano beads as a basis for biochip development. The detection of molecular recognition (the interaction of complementary or affinity-linked biomolecules) with GMR has been shown. The sensor element can be made of a fraction of micron in size and can in principle provide the detection at the level of a single molecular interaction (Gaster et al, 2009). Yet, the GMR technology for biosensing is regarded as long-term development owing to the need to improve either sensitivity or highly spatial resolution. It requires precise manipulation of magnetic beads that must be transported to the sensor location. This approach makes the technology very specific, not suitable for a wider range of application, and in fact prevents its transfer from laboratory to end-user. GMI offers at least an order of magnitude higher magnetic field resolution (down to 10 PicoTesla) than GMR but is larger in size with a single sensing area limit of about 5μm×50μm at frequencies of 20-250MHz. Integration of both GMR and GMI sensing concepts could be a possibility.

The discovery of GMI effect in 1993 (Panina & Mohri, 1994; Beach & Berkowicz, 1994) had a strong impact on the development of micro magnetic sensors operating in the nano-Tesla

range (Zhukova et al, 2009; Mohri et al, 2001, 2002). In certain soft magnetic materials, such as composites of amorphous thin wires, the impedance change (GMI ratio) is in the range of more than 100 % in the MHz frequency band for the external magnetic fields of 0.1mTesla. One of the main activities in improving GMI technology is devoted to developing miniature GMI systems preserving high sensitivity. This could be realised in ultrathin amorphous/nanocrystalline wires and multilayer structures with inner silver/gold lead. In particularly, the modelling results for CoFeSiB/Au/CoFeSiB multilayers with in-plane size of 20μm×100μm and thickness of 1μm demonstrate the GMI ratio of more than 300% at 350 MHz (Morikawa et al, 1997; Hika et al, 1994). Further miniaturisation and high GMI ratios are proposed to be achieved employing structures having a special spiral type of anisotropy (Panina et al, 2001). GMI sensors and particular their arrays provide the needed sensitivity for magnetic cardiography (MCG) and some laboratories have already reported successful detecting cardiac signals with the use of GMI (Uchiyama et al, 2009). An MCG allows details of the localised electrical activity of the heart to be revealed, enabling accurate diagnosis of heart conditions. The development of room temperature MCG would be of great importance for wide practical use.

We further will discuss the use of non linear magnetisation of magnetic labels for their sensitive detection. Magnetic labels or carriers, also referred to as microspheres, microbeads and nanoparticles, have found wide-ranging scientific and clinical application in biotechnological and biomedical research (Haukanes & Kvam, 1993), most notably in the areas of bioseparations, molecular biology and drug delivery. The labels used are non-remanent paramagnetic or superparamagnetic beads. The magnetic material within the label exists as small particles (usually iron oxide), having random moments. A conventional magnetic sensor system relies on the alignment of these moments within the label to produce a measurable fringe field. On the other hand, the magnetisation of such magnetic particles is a nonlinear function of external magnetic field and capable of generating high frequencies harmonics having high signal to noise ratio, thus, high detection sensitivity.

Therefore, the purpose of this chapter will be to promote relatively new magnetic sensing technologies for use in biomedical field. GMI and MPS can offer very high sensitivity (sub nano-Tesla range), low cost, with the benefit of a portable operation. In many areas of medical applications, such as MCG and magnetic immunoassays, the importance of these sensing technologies cannot be overestimated as they may provide relatively simple room-temperature tests, which could be realised in any general hospital, unlike such expensive methods as SQUID magnetometry.

2. SQUID magnetometers for biosensing applications

SQUID instrument depends on the effects of magnetic fields on circuits containing superconducting (Josephson) junctions. The temperature at which these operate is traditionally at about 4° Kelvin which is the temperature of liquid Helium. A Josephson junction, which is the essential part of a SQUID device, is effectively a weak link between two superconductors that is capable of carrying supercurrents below a critical value. There are two types of SQUIDs: rf SQUIDs and dc SQUIDs. In both types, the device consists of a superconducting ring interrupted by one (rf) or two (dc) Josephson junctions. The difference between the two is in the nature of the biasing current being an rf or a dc. In either type, the properties of the Josephson junction cause the impedance of the ring to vary periodically as a function of the magnetic flux crossing the ring. With the use of a lock-in detector to

measure the impedance, SQUIDs can operate as flux-to-voltage converters with highest magnetic sensitivity of any magnetometer in existence. Recently, with the discovery of high-temperature superconductors, SQUID systems at liquid nitrogen temperatures (e.g. 70° Kelvin) have been built although the noise level is significantly higher than that of the liquid helium systems (Mahdi & Mapps, 2000). A typical principle of operation is to detect two magnetic signals at different distances from the source and arrange for these to be in opposition around a local supercooled circuit. This 'gradiometer' approach eliminates most of the noise – caused by spurious magnetic fields originating from, for example, electrical devices or natural (geomagnetic) sources. A typical unshielded laboratory has a noise level in the dc to ten hertz frequency region of about 10^{-7} Tesla so a magnetically screened environment is usually required for these studies. The basic requirement has been for a noise level of the measuring environment to be lower than the sensor limit and this has caused the design and construction of sophisticated screened rooms in hospitals environments (Ter Brake, 1991). The screened rooms currently in use employ large amounts of mu-metal and are generally built as hospital rooms where patients can walk in and sit under comparatively large SQUID detector systems. For smaller systems this will not be necessary since screening is actually only needed in the detection zone, for example around the head. For this a screened 'hat' is envisaged which will be at much lower cost. Also various techniques are available for providing noise cancellation such as at the National Physical Laboratory, Teddington, U.K. where 'negative' noise is generated and added to the noise in the measurement zone by a Helmholz coil system (Hall, 2001).

A single measurement of a field, for example, near the head has only a very limited value in neural analysis of the brain. Therefore, multiple SQUID systems have been devised and used in an attempt to build up a picture of the increased neural brain activity that results, for example, when the biological subject of the study has been stimulated in some way. The development of multiple SQUID systems has also led to an acceleration of research on MEG systems having, typically, 150 SQUID sensors arranged in a framework around the head. A great deal of research on this has been done by Professor Ueno in Japan (Iramina et al, 2001; Iramina et al, 1997). Similar multiple detection systems have also been developed for EEG in the past and an interesting comparison can be made with MEG.

3. GMR for biosensing applications

Giant magnetoresistive (GMR) sensors as biosensors are mainly developed in conjunction with magnetic immonoassays. Magnetoresistive-based biochips were first introduced in 1998 by the Naval Research Laboratory (NRL) and since then an increasing number of research laboratories and companies have been developing such systems (Graham et al., 2004; Megens & Prinz, 2005; Tamanaha et al., 2008; Xu et al., 2008, Martinsa et al, 2009). The use of small magnetic particles or beads in biomedical sciences has increased significantly in recent years (Haukanes & Kvam, 1993). Integration of sensor design with magnetic-particle and assay development is a significant part of this research. Magnetic labels usually are superparamagnetic or non-remanent ferromagnetic in nature, with nano- or micrometer dimensions, and can attach to the target biomolecules. Under an applied magnetic field these particles or beads acquire a moment and their fringe field can induce a change in resistance of the magnetoresistive sensor, enabling biomolecular recognition detection.

The change in material resistance, which occurs when the magnetisation changes from parallel, with respect to the direction of current flow, to transverse is known as anisotropic

magnetoresistive effect (AMR). AMR is present in ferromagnetic alloys such as NiFe, NiFeCo, but the resistance change is small. A large change in resistance up to 70% (Baibich et al, 1988) is based on the spin dependent interfacial and bulk scattering asymmetry that is found for spin-up and spin-down conduction electrons crossing ferromagnetic–nonmagnetic–ferromagnetic multilayer structures, where the parallel or antiparallel alignment of the ferromagnetic layers can be engineered. Then, the resistance of two thin ferromagnetic layers separated by a thin nonmagnetic conducting layer can be altered by changing the moments of the ferromagnetic layers from parallel to antiparallel. Layers with parallel magnetic moments will have less scattering at the interfaces, longer mean free paths, and lower resistance. Layers with antiparallel magnetic moments will have more scattering at the interfaces, shorter mean free paths, and higher resistance. For spin-dependent scattering to be a significant part of the total resistance, the layers must be thinner than the mean free path of electrons in the bulk material. For many ferromagnets the mean free path is tens of nanometers, so the layers themselves must each be typically thinner than 10 nm. There are various methods of obtaining antiparallel magnetic alignment in thin ferromagnet-conductor multilayers. The structures currently used in GMR sensors are unpinned sandwiches, antiferromagnetic multilayers and spin valves.

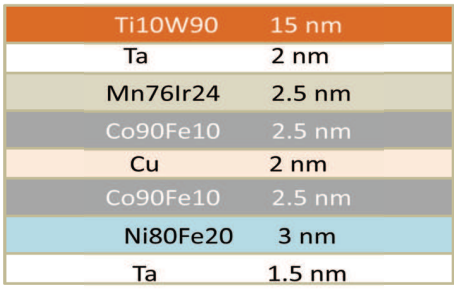

Fig. 2. Spin-valve multilayer system.

The structure of the spin-valve sensor used in (Martinsa et al, 2009) is shown in Fig. 2. The pinned and free layers are deposited with the easy axes in parallel orientation. The shape anisotropy is then used to rotate the easy axis of the free-layer at 90◦ to get a linear response. The sensor element is patterned by direct write laser photolithography and ion milling, resulting in U-shaped sensors with a final active area of 2.5×80 μm^2. Patterned sensors have an average magnetoresistance of 7.5%. A differential sensor set-up uses a reference sensor in the Wheatstone bridge architecture to enable thermal and electrical (mains) drift compensation between a biologically active sensor and a biologically inactive sensor.
The fields required to change the magnetisation direction in one of the layers could be in kOe range resulting in a reduced sensitivity. When used as biosensors, the needed sensitivity was obtained thanks to the combination of detection and manipulation of magnetic particles. The secret of the sensitivity improvement lies within the location of the magnetic markers on the chip via active guiding of magnetic particles using on-chip generated magnetic forces. First, a sandwich assay is built up on the device surface, followed by labelling with magnetic particles. Then, the bound magnetic particles are released and transported to the position that theoretically gives rise to the maximal signal, ensuring the most sensitive detection. This process is schematically demonstrated in Fig. 3.

Magnetic label detection has been accomplished by using different types of integrated GMR sensor designs, such as stripes, meander, spirals, and serpentine-shaped GMR sensors. Different shapes of GMR sernsors were tried in an attempt to optimize the sensor active surface, averaged stray magnetic fields and on-chip manipulation and transport of magnetic beads.

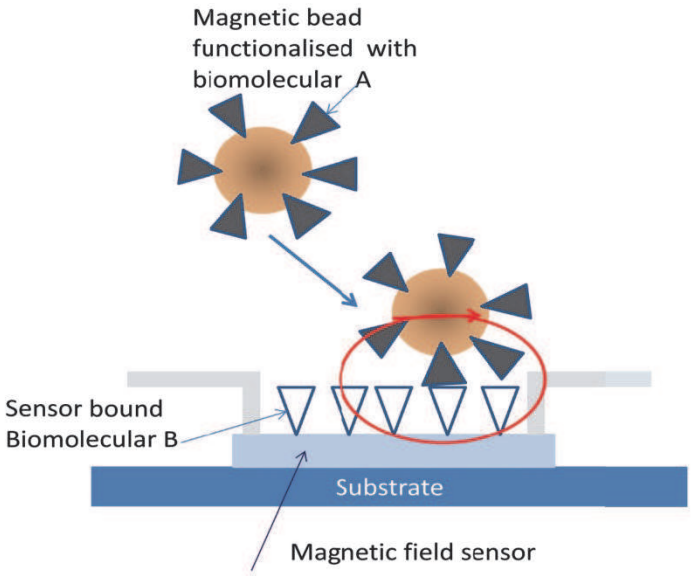

Fig. 3. Schematic of a biochip which is composed of GMR sensors, an array of probe biomolecules (biomolecules B of known identity) immobilized onto the surface of the sensors, magnetic labels functionalized with target biomolecules (A) that bind to the sensor surface through biomolecular recognition. The magnetic fringe field resulting from the magnetic moment of the label induced by an on-chip applied magnetic field changes the resistance of the sensor, resulting in a voltage signal.

Typical target analyte resolutions today are near 1pM for passive detection (INESC MN) using spin valve sensors (few nT/Hz $^{1/2}$) at thermal background. The sensor element covers partially the probe immobilization area (few hundred μm^2). Increase in sensitivity is being pursued by moving towards low noise magnetic tunnel junction based platforms. INESC MN has demonstrated field resolutions down to few tens pT/ Hz ^{½} (Martinsa et al, 2009). Although single molecule process detection is within reach by reducing the sensor size towards the magnetic label dimension, for practical applications, the challenge resides in increasing sensitivity to allow detection of few sub 100 nm labels with a dynamic range up to few thousand labels on a point of care portable device. Furthermore, the use of labelled targets has allowed the use of current lines for magnetically assisted hybridization. INESC-MN has been exploring this ability to enhance the sensitivity and specificity via active guiding of magnetic beads using on-chip generated magnetic forces, hoping to reach detection sensitivity into the fM range (Martinsa et al, 2009). This approach makes the technology very specific, not suitable for a wider range of application, and in fact prevents its transfer from laboratory to end-user.

4. Biosensor based on non linear magnetization detection

One of the most promising approaches in developing magnetic biosensors associated with the use of magnetic labelling is based on non-linear magnetisation of magnetic beads. Non-linear magnetisation processes result in the generation of higher order harmonics which can be detected and discriminated for use in remote sensing and monitoring (Ong & Grimes, 2002). Typically, as biological labels, nanosized magnetic particles are used which are in a single domain state and demonstrate superparamagnetic behaviour with an essential non-linearity. The non-linear magnetisation permits easy discrimination of these particles from surrounding paramagnetic materials and their reliable detection by high harmonic spectrum techniques for many biological applications. The magnetization of non-interacting particles obeys the Langevin function as shown in Fig. 4. If a system of such magnetic particles is excited by a harmonically oscillating magnetic field of frequency ω its magnetisation response $M(t)$ is non-linear and contains integer multiples of ω, so-called higher harmonics. This non linear magnetisation response can be detected inductively and evaluated spectroscopically. Therefore, this detection method is often referred to as magnetic particle spectroscopy (MPS). The induced inductive voltage is proportional to the rate of the magnetisation change:

$$V(t) \propto \frac{\partial M}{\partial t}$$

This represents the measurable quantity which also reflects the magnetisation response's degree of distortion: it is clearly not harmonic anymore. The excitation magnetic field, the response functions and the voltage signals are depicted in Fig. 5.

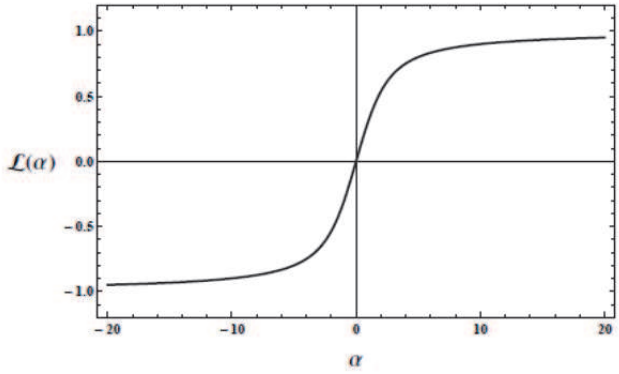

Fig. 4. Plot of the Langevin function representing the relative magnetization of a system of noninteracting and freely rotatable magnetic moments.

The next step is to obtain the detected signal's frequency spectrum, i.e. resolving the harmonic contributions and their amplitudes. Therefore, the time signal has to be transformed into the frequency domain by a Fourier transformation. Generally, the exact calculation of Fourier series coefficients is too difficult or impossible. Instead, $V(t)$– no matter if it was gained synthetically (analytically/ numerically) or in an experiment – is analysed numerically using a discrete Fourier transformation (DFT). Therefore, $V(t)$ has to be sampled with a specific rate f_{sample}, yielding a set of data points $V_i(t_i)$. Then, DFT transforms $V_i(t_i)$ into $A_i(\omega_i)$, i.e. it resolves the complex amplitude A_i for a specific frequency ω_i.

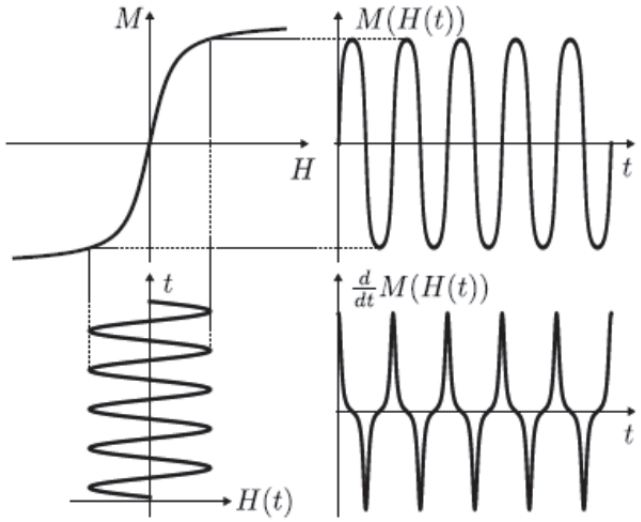

Fig. 5. Harmonic magnetic excitation *H(t)* of superparamagnetic particles. Transfer function *M(H)*(top left). Magnetization response *M(t)* (top right). Response's time derivative, which is proportional to measurable voltage *V(t)* (bottom right).

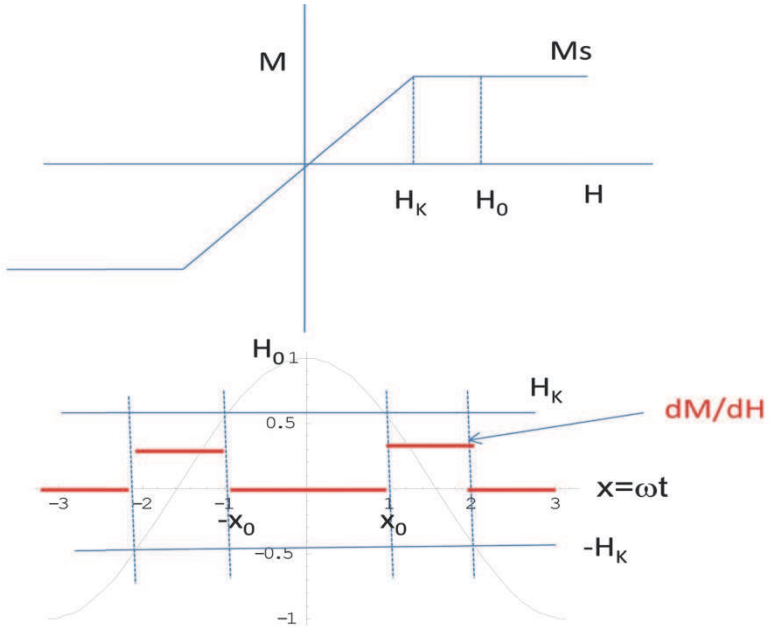

Fig. 6. Idealised response function $M(H)$: linear for $|H| < H_K$ and constant for $|H| > H_K$ (top). Magnetic excitation and step-wise susceptibility $\partial M/\partial H$ (bottom).

For illustration of the method, an idealised response function: linear with saturation, as shown in Fig. 6 is considered. The magnetization saturates when the magnetising field exceeds a characteristic value, denoted by H_K. Suppose, that the magnetising field is changing as $H = H_0 cos\omega t$. Then, the voltage signal is proportional to

$$V \propto \frac{\partial M}{\partial H}\frac{dH}{dt} = H_0\omega \sin\omega t \frac{\partial M}{\partial H} \tag{1}$$

The case of interest is when the amplitude of the magnetising field is sufficient to reach the saturation: $H_K < H_0$ for which $\partial M/\partial H$ is a step-wise function:

$$\frac{\partial M}{\partial H} = \begin{cases} \frac{M_S}{H_K} = \chi, & x_0 < x = \omega t < \pi - x_0, \ x_0 = \cos^{-1}(H_K/H_0) \\ 0, & otherwires \end{cases} . \tag{2}$$

Since the voltage signal in (1) is an odd function of time, the Fourier spectra will be represented by sin-series:

$$V(x) = \sum_{n=1}^{\infty} A_n \sin nx\,, \qquad -\pi \le x = \omega t < \pi. \tag{3}$$

In this case, the harmonic coefficients A_n can be expressed analytically for any n:

$$A_1 \propto \frac{2H_0\omega\chi}{\pi}\int_{x0}^{\pi-x0} \sin x \ \sin x dx = \frac{H_0\omega\chi}{\pi}[\pi - 2x_0 + (\sin 2x_0)]\,. \tag{4}$$

$$A_{2k+1} \propto \frac{H_0\omega\chi}{2\pi}\left[\frac{\sin 2k(\pi - x_0) - \sin 2k(x_0)}{k} - \frac{\sin 2(k+1)(\pi - x_0) - \sin 2(k+1)(x_0)}{(k+1)}\right]. \tag{5}$$

In (5), $= 1,2, \ldots$. The spectra calculated from (4) and (5) for different values of parameter $h = H_0/H_K$ which reflects the degree of non-linearity are shown in Fig. 7.

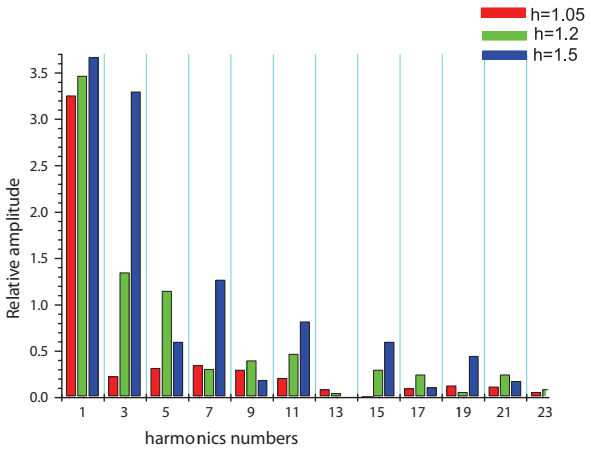

Fig. 7. Harmonic spectra for magnetisation response function of Fig. 6 and described by Eqs. (1), (2).

It is seen that certain high –order harmonics preserve relatively large values (as harmonics 19 and 21 for $h = 1.5$) and can be used for determination of the magnetic particle concentration. It is also interesting to notice that the spectra have specific characteristics depending on parameter h, such as non monotonic decrease with increasing n, which can be used for magnetic particle discrimination in multiparameteric analysis. The spectra will change dramatically in the presence of off-set dc magnetic field. Utilising spatially dependent off-set field, imaging techniques with non-linear magnetic particles can be developed (Gleich & Weizenecker, 2005; Weizenecker et al, 2009). The achieved resolution is well below 1 mm and the method has the potential to be developed into an imaging method characterised by both high spatial resolution as well as high sensitivity.

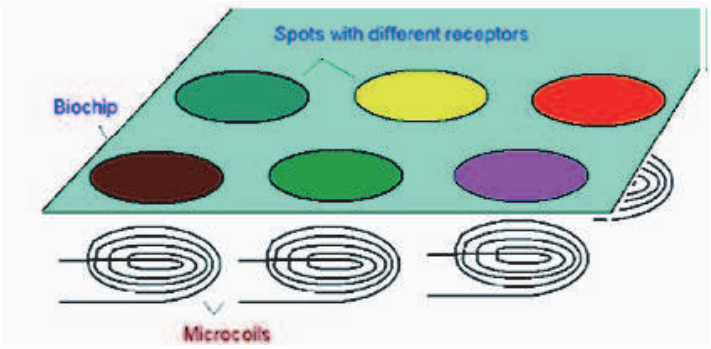

Fig. 9. Arrays of inductive coils and immobilization zones for multi component immunoassay.

Further, magnetic particles with non-linear response can be subjected to multi tone excitation. It was proposed to use the interrogation magnetic field with two frequencies, ω_1 and ω_2, the first one being considerably higher (Nikitin et al, 2007, 2008). The amplitude of the lower frequency tone is chosen high enough to get a strong non-linearity of $M(H)$. For example, this component may periodically 'switch' on and off the capability of magnetic particles to change the magnetisation. When the particle can be further magnetised, the higher frequency component ω_1 contributes to the resulting induction signal. As a result, the response signal $V(t)$ is non-linearly modulated by both frequencies. The spectral response is measured at combinatorial frequencies $\omega_{nm} = m\omega_1 + n\omega_2$, where m and n are integers. This technique results in much higher SNR than in the case of a single-tone excitation. It was successfully applied for multi-component analysis using coil-arrays and zones with different immobilised agents as shown in Fig. 9. Several sensing configurations for superparamagnetic particle detection have been developed in a wide linear dynamic range (3 ng–70 mg) in the volume of 0.1–0.4 cm^3. The sensitivity of this type of magnetic immunoassays at the level of 0.1 ng/ml for soluble proteins of LPS from F. tularensis has been demonstrated (Nikitin et al, 2007).

5. Giant magnetoimpedance (GMI)

Giant magnetoimpedance (GMI) has at least one order of magnitude higher sensitivity than GMR and can be developed for measurements of magnetic fields from human body such as the fields from heart and muscles, as well as for magnetic immunoassays.

5.1 Basic principles of GMI

First experiments on GMI dated to 1993 were obtained with amorphous magnetic wires and ribbons utilizing a simple concept of measuring an ac voltage in the presence of a dc magnetic field H_{ex} applied in parallel with the current (Panina & Mohri, 1994; Beach & Berkowicz, 1994). For wires with the composition $(Co_{0.94}Fe_{0.06})_{72.5}Si_{12.5}B_{15}$ having almost zero magnetostriction of -10^{-7} the impressive sensitivity (the impedance ratio per a unit of magnetic field) of up to 100%/Oe at MHz frequencies was quickly realised. Since then, the range of materials exhibiting large and sensitive GMI rapidly expanded including nanocrystalline wires and ribbons, as well as more sophisticated materials as multilaered wires and films (Vazquez et al, 2011; Panina, 2009; Phan & Peng, 2008; Knobel & Pirota , 2002). GMI can be considered as a high frequency analogy of giant magnetoresistance. However, the origin of GMI lies in classical electromagnetism and can be understood in terms of the skin effect in conjunction with the transverse magnetization induced by a passing ac current $i = i_0 exp(-j\omega t)$. For some simple geometries and magnetic structures the impedance can be approximated by an analytical form valid for any frequency. Thus, for a wire with a circular cross section and circular domain structure placed in an axial magnetic field H_{ex} and carrying a current i, the impedance is given by (Panina et al, 1994):

$$Z = \frac{R_{dc}(ka)J_0(ka)}{2J_1(ka)} \tag{6}$$

$$k = \frac{1+j}{\delta_m}, \quad \delta_m = \frac{c}{\sqrt{2\pi\sigma\omega\mu_\varphi}} \tag{7}$$

In (6) and (7), R_{dc} is the dc resistance of the wire, a is the wire radius, J_0, J_1 are the Bessel functions, σ is the conductivity, c is the velocity of light (cgs units are used), δ_m is the penetration depth depending on the wire circular permeability μ_φ, $j = \sqrt{-1}$. The circular permeability should be defined considering the full ac permeability tensor $\hat{\mu}$ from the constituent equation: $b_\varphi = (\hat{\mu}\boldsymbol{h})_\varphi = \mu_\varphi h_\varphi$, which connects the ac magnetic field $\boldsymbol{h}$ and induction $\boldsymbol{b}$. Equation (6) is valid if the induced axial induction $b_z = 0$. For high frequencies, when the skin depth is smaller than the wire radius, the impedance becomes inversely proportional to δ_m, and hence, proportional to $\sqrt{\mu_\varphi}$.

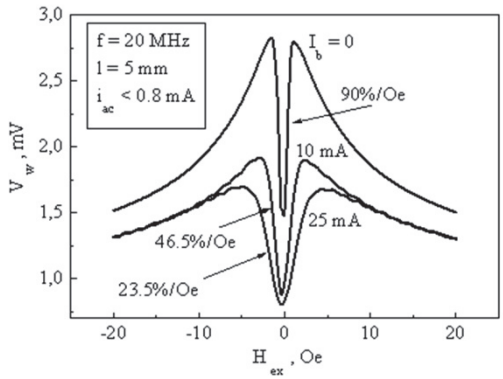

Fig. 10. MI plots in glass-coated CoFeNiSiB wires having a metal core diameter of 48 μm and the total diameter of 50 μm with a dc current as a parameter

Therefore, the changes in permeability which could be few orders of magnitude when the dc magnetisation is rotated from circular direction to the axial direction can be detected by measuring the wire impedance (Garcia et al, 2000). The example of GMI characteristics in amorphous wires is given in Fig. 10 showing the sensitivity up to 90%/Oe. The samples are glass coated wires with well established circumferential anisotropy.

In the MHz frequency range, the parameter μ_φ in general has contributions from domain wall displacements and moment rotation. For sensor applications, it is preferable to eliminate the domain structure in order to avoid Barkhausen jumps noise. For wires with a helical type of anisotropy, this can be done by applying a dc bias current I_b as shown in Fig. 10. However, this current contributes to magnetic hardness so the sensitivity reduces and the value of I_b should be carefully optimized.

For a complicated magnetic configuration which support modes with axial induction b_z, equation (6) becomes invalid and asymptotic or numerical methods should be used to calculate the impedance at arbitrary frequency even for a wire with a circular cross-section (Makhnovsky et al, 2001). However, at high frequencies when the skin effect is strong ($a \gg \delta_m$), the following asymptotic form for the local surface impedance parameter $\varsigma_{zz} = e_Z/h_\varphi$, which is the ratio of the tangential components of electric and magnetic fields at the surface, can be used:

$$\varsigma_{zz} = \frac{c(1-j)}{4\pi\sigma\delta_0}\left(\sqrt{\tilde{\mu}}\, cos^2\theta + sin^2\theta\right), \quad \delta_0 = \frac{c}{\sqrt{2\pi\sigma\omega}} \tag{8}$$

In (8), the angle θ is the angle between the dc magnetisation and the current direction. The magnetic parameter $\tilde{\mu}$ is the effective transverse permeability with respect to the dc magnetisation. Equation (8) demonstrates clearly the role of the dc magnetisation in determining the high frequency impedance and is very useful for designing the materials with required GMI characteristics.

Substantial amount of works on GMI have been devoted to the asymmetric effects (Panina et al, 2004; Ueno et al, 2004; Delooze et al, 2003; Panina et al, 1999). In the case of sensor applications, the linearity of GMI is an important feature. On the other hand, the GMI characteristics presented in Fig. 10 are not only non-linear, but also shaped in a way that the operation near zero-field point can present serious problems. Generally, a dc bias field is used to set properly the operating point on the GMI characteristics, which can be regarded as producing asymmetry with respect to the sensed field H_{ex}. Therefore, for linear sensing the asymmetrical magnetoimpedance (AMI) is of great importance. There are mainly two ways to realise AMI. The first one is due to asymmetrical static magnetic structure, which can be established in multilayers involving a hard magnetic layer or a layer with a helical anisotropy. The other method is based on the dynamic cross-magnetisation processes. The linear GMI characteristics can be also obtained when detecting the induced voltage from the coil mounted on GMI element when it is excited by a high frequency current (Sandacci et al, 2004). This is based on off-diagonal component of the impedance. This configuration was adopted by Aichi Steel for the development of miniature compass for mobile communication (Mohri & Honkura , 2007; Honkura, 2002).

The condition of a strong skin effect to obtain large GMI may not be required for multilayered systems having an inner conductive lead. If its resistance is considerably smaller than the resistance of the magnetic layers the current mainly flows along the conductive lead. With these assumptions, the expression for the impedance can be written in the form (Hika et al, 1996):

$$Z = R_c - \frac{j\omega\Phi}{ci} \tag{9}$$

where R_c is the resistance of the inner conductor and Φ is the total transverse magnetic flux generated by the driving current i in the magnetic layers. The second term in (9) can be made much larger than R_c in a wide frequency range from MHz to GHz bands in structures with Cu, Ag, Au inner leads and soft magnetic amorphous outer layers of submicron cross section. In particular, multilayered thin films would be of interest for sensing applications in the context of miniaturisation and compatibility with integrated circuit technology.

5.2 Magnetic wires for GMI

Thin amorphous ferromagnetic wires of Co-rich compositions having a negative magnetostriction are very popular for GMI applications (Vazquez et al, 2011; Mohri et al, 2009; Zhukov & Zhukova, 2009). In the outer layer of the wire, an internal stress from quenching coupled with the negative magnetostriction results in a circumferential anisotropy and an alternate left and right handed circular domain structure (Takajo et al, 1993). In this case, the circular magnetization processes determining the GMI behaviour are very sensitive to the axial magnetic field. Along with this, special types of anisotropy as a helical one can be established in the outer layer by a corresponding annealing treatment, which results in unusual asymmetric GMI behaviour. Many experimental results on GMI and designed magnetic sensors utilise amorphous wires of $(Co_{1-x}Fe_x)SiB$ compositions with $x < 0.06$ to decrease the magnetostriction down to -10^{-7} and the characteristic saturation magnetic fields down to few Oe.

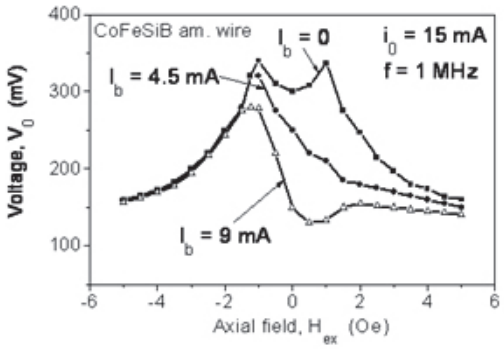

Fig. 11. AMI plots in torsion annealed wires (280 turn/m, 500C) with I_b as a parameter.

Currently, there are basically two methods of wire fabrication techniques. The first one utilises in-water-spinning method for which as-cast wires have a diameter of 125 microns (Ogasawara & Ueno, 1995). The wires then cold drawn down to 20 - 30 μm, and finally annealed under stress to established a needed anisotropy. In the case of negative magnetostrictive wires, annealing under a tension induces a circumferential anisotropy for which the GMI plots shown in Fig. 10 are typical. If the wire is annealed under torsion stress a helical type of the anisotropy is introduced which is important for asymmetrical GMI as shown in Fig. 11 (Panina, 2004).

Fig. 12. Sketch of a glass-coated wire.

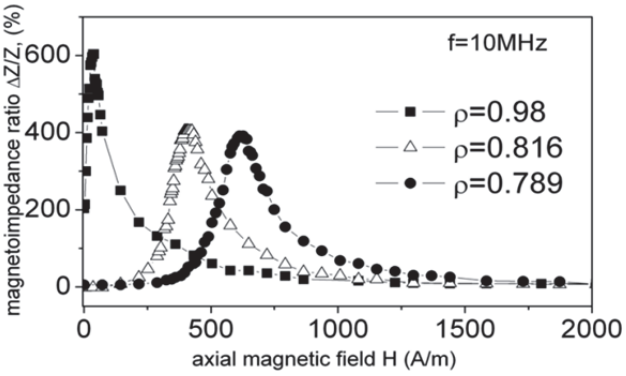

Fig. 13. GMI plots in $Co_{67}Fe_{3.85}Ni_{1.45}B_{11.5}Si_{14.5}Mo_{1.7}$ glass-coated wires for different values of ρ. d_w is about 22 μm.

The other technique produces amorphous wires in a glass cover (see Fig. 12) by modified Tailor method which is also referred to as Talor-Ulitovsky method (Zhukov et al, 2009; Larin et al, 2002; Zhukov et al, 2000; Chiriac et al, 1996). The method is based on drawing a thin glass capillary with molten metal alloy. The diameter of the metal core is ranging between 1-50 microns and even submicron cross section size is possible (Zhukov et al, 2008). In this case, different temperature expansion coefficients of glass and metal alloy result in a longitudinal tensile stress, which is needed for the circumferential anisotropy. The value of this stress and induced anisotropy depends on the wire composition and ratio $\rho = d_w/D_w$ of the metal core diameter d_w to the total diameter D_w. This is a simple one-step process allowing a strict control of properties in as-cast state and optimisation of the GMI characteristics. Figure 13 (Zhukova et al, 2002) shows the GMI ratio vs. external field for different values of ρ. For a very thin glass layer, the GMI ratio reaches 600% for a field of about 1 Oe at a frequency of 10 MHz. This is the best result obtained so far for any GMI system.

5.3 Multilayered films for GMI

Magnetic/metallic multilayers are especially important for miniaturisation of GMI elements and realising arrays of GMI sensors. The basic structure consists of an inner conductive lead (M) and two magnetic layers (F) as shown in Fig. 14. The magnetic layers could be made of the same alloy, yet, they can be produced with different magnetic anisotropies. In particular, for asymmetric magnetoimpedance the anisotropy axes have to be directed at an angle $\pm\alpha$ to the long (current) axis, respectively for the upper and lower magnetic layers. Such anisotropy can be induced, for example, by current annealing in the presence of a longitudinal field.

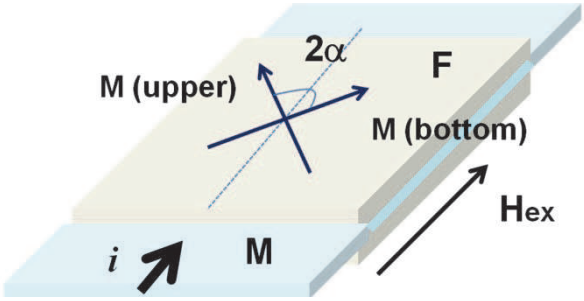

Fig. 14. Sketch of multilayered films. The case of crossed magnetic anisotropy axes in the bottom and top layers makes it possible to obtain almost linear GMR characteristics .

If the edge effects are neglected (i.e., the film is treated as infinitely long in the plane directions) equation (9) for the impedance becomes (Hika et al, 1996):

$$Z = R_c(1 - 2j\tilde{\mu}\frac{d_1 d_2}{\delta_c^2}) \tag{10}$$

Here $2d_1, d_2$ are the thicknesses of the inner and outer layers, respectively, δ_c is the skin depth in the metallic inner lead. Expression (10) shows that the GMI ratio in the sandwich film can be very large even at relatively low frequencies when the skin effect is not substantial, and has a linear dependence on the permeability. This conclusion can be illustrated as follows. At a frequency of 10 MHz, taking $d_1 = d_2 = 0.5\,\mu m$ and $\sigma_{Cu} = 2 \cdot 10^{18} s^{-1}$(conductivity of Copper), we get $d_{1,2}/\delta_c = 0.045$ (so, the skin effect is weak). A typical low-frequency change in the permeability $\tilde{\mu}$ (having a rotational mechanism) under the application of the field equal to the anisotropy field is from 1 to 500; then, the impedance varies over 200% according to (10). In the case of a similar magnetic layer of submicron thickness, the change in the impedance would not be noticeable at these conditions since the skin effect is week. A considerable enhancement of the GMI effect in multilayers can be achieved by insulator separation between the conductive lead and the magnetic films, which prevents layer diffusion and further decreases the DC resistance. A CoSiB/SiO_2 /Cu/SiO_2/CoSiB multilayer of total thickness of 7 microns exhibited the GMI ratio of 620% for 11 Oe (Morikawa et al, 1997).

For a practical device design, the effect of in-plane sandwich width on GMI has to be studied. If the edge effect is neglected (approximation of an infinite width), the magnetic flux generated by the current flowing along the inner lead is confined within the outer magnetic layers. In a sandwich of finite width 2*b*, the flux leaks across the inner conductor (Panina et al, 2001). This process eventually results in the considerable drop in GMI ratio, if the film width is smaller than some critical value b^* depending on the transverse permeability and the thicknesses of the magnetic and conductive layers. This process is similar to that resulting in a drop in the efficiency of inductive recording heads and magnetoresistive thin-film devices. In the low-frequency limit, $b^* = \sqrt{d_1 d_2 \tilde{\mu}}$. Typical parameters for the structures of interest are $d_1 \sim d_2 \sim$0.1-0.5 μm, $2b \sim$10-50 μm and $\tilde{\mu} \sim 10^3$. This gives the value of $b^* \sim$3-15 μm, which is comparable to the half-width, suggesting that the size effects cannot be neglected. The results of modelling the maximum of the GMI ratio vs. frequency, with a width *b* as a parameter are shown in Fig. 15. It can be concluded, that even for films narrower than 25 microns very high values of the GMI ratio can be obtained at higher frequency region which was confirmed experimentally for NiFe/Au/NiFe films (De Cos et al, 2005).

The most interesting results on thin film GMI are obtained in amorphous films CoFeB/Cu/ CoFeB with cross-anisotropy (Delooze et al, 2003; Ueno et al, 2000). The films were made on a glass substrate by dc sputtering. During the deposition, a constant magnetic field of 200 Oe was applied in the transverse direction to the GMI element in order to add uniaxial anisotropy. Finally, crossed anisotropy was induced in the sample by current annealing (30 mA) in a longitudinal field of 11.8 Oe at a temperature of 215°C. The anisotropy axes in the upper and bottom layers are at approximately 67° to the long axis, which was estimated from the DC magnetization loop measurements. Applying a bias current produces highly asymmetrical GMI plots as shown in Fig. 16 (Delooze et al, 2004). The differential characteristic from two oppositely biased GMI films is also given, demonstrating a near linear region in the field interval of ± 5 Oe.

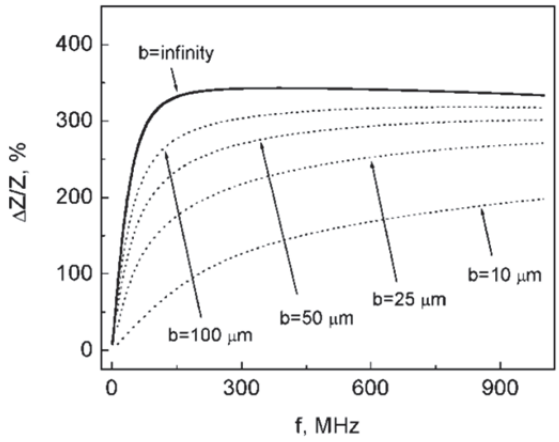

Fig. 15. Maximum of GMI ratio calculated at the anisotropy field, vs. frequency at different values of width b. $2(d_1+d_2) = 1\mu m$, conductivity ratio is 50.

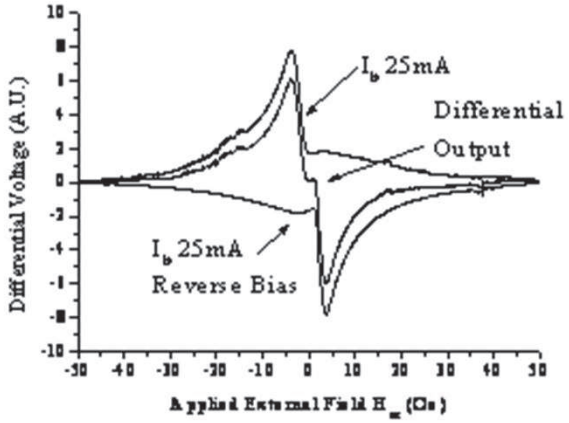

Fig. 16. GMI characteristics in $Co_{70.2}Fe_{7.8}B_{22}$ /Cu/ $Co_{70.2}Fe_{7.8}B_{22}$ films with a DC bias current of 25 mA and their differential output. Magnetic films are amorphous. $d_1 = d_2 = 0.5\ \mu m$.

6. GMI sensor design and biomedical applications

There is a number of high frequency circuits designed to drive GMI elements. One of the most successful solutions utilises a pulse excitation of the GMI element with the help of C-MOS digital circuits(Mohri & Honkura, 2007; Mohri et al, 2002, Shen et al, 1997). The circuit with a C-MOS IC multivibrator as shown in Fig. 17 produces sharp-pulsed current of duration 5–20 ns.

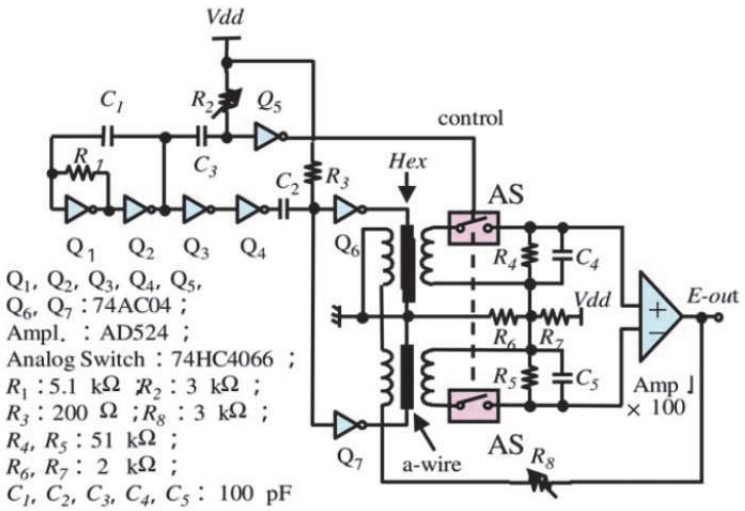

Fig. 17. High-stability CMOS IC with analog-switch type GMI sensor circuit

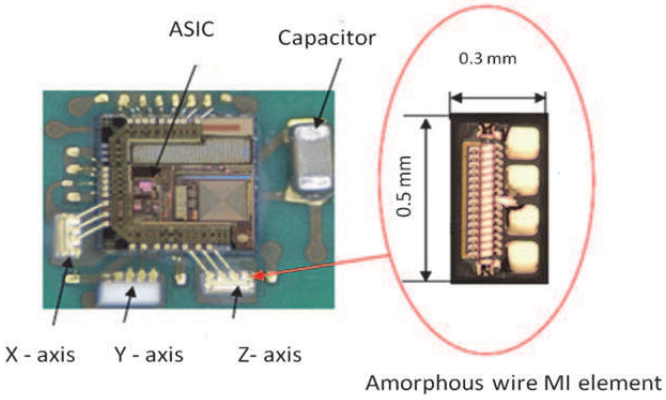

Fig. 18. Three axis electric compass using amorphous wire GMI element.

Pulse excitation provides: simplicity of electronic design, low cost components, and reasonably good stability since C-MOS multivibrator oscillation frequency almost does not depend on the impedance characteristics of the GMI elements. Power consumption of this circuit is also small (10mW). In addition, such pulsed current involves both high frequency

(20–100 MHz) and low (quasi-DC) harmonics. Therefore, it can be ideally used for the asymmetrical GMI requiring a dc or ac bias. Generally, the method provides the field detection resolution of 10^{-4} Oe (10nT) for dc fields and 10^{-6} Oe (100pT) for ac fields. Recently, Aichi Steel Co. has developed GMI-sensor IC-chip (shown in Fig. 18) for mobile phone electronic compass for mass production (Mohri & Honkura, 2007). The restrictions in the field resolution at that level are not due to the intrinsic limitations of advanced GMI elements, but related with the circuit performance. For biomagnetic sensing with GMI further improvements in circuitry are needed, which was achieved with the use of CMOS timer circuit as the multi-vibrator oscillator to effectively reduce circuit noise. In a shielded environment and differential signal amplification, the rms noise was estimated as 3 $pT/Hz^{1/2}$ at 1 Hz (Uchiyama et al; 2009).

In another approach to GMI sensor design, a single frequency excitation is used (Delooze et al, 2005; Yabukami et al, 2004; Yabukami et al, 2001). The sensor measurement system represents a single frequency network analyzer to measure the magnitude of the incident reflected power produced by a mismatch in the complex impedance between the source and load. Typically, GMI thin-film elements are used in this scheme. The incident power or carrier is produced by a Surface Acoustic Wave (SAW) filtered crystal oscillator designed for low power, portable applications. The reflected power is separated from the incident power by means of a directional coupler based on an active op-amp design which provides non-magnetic coupling approach to lower noise. When the impedance of the GMI element matches the impedance of the source (50Ω) the maximum amount of power is transferred to it. With no external field the carrier is suppressed by 60dB. An AC external field causes variation in the 50Ω impedance of the sensor element, which is measured as an AM modulation on the suppressed carrier in the reflected incident power. This is then demodulated, filtered, amplified and measured. For high frequency field detection (>10MHz), the resolution is in the range of pT. Low frequency phase noise (1/f) of the oscillator limits the performance of the sensor at frequencies lower than 1 kHz. A technique to overcome this problem is to firstly modulate (chop) the low frequency AC field to be measured with a locally produced high frequency field (1 to 5 kHz). The second local modulation field shifts the measurement field of interest to a higher frequency offset from the local modulation. This allows the measurement of the low frequency field in the spectrum of the oscillator that is not affected by the phase noise. The achieved ac biased field performance is as following: a 20 Hz field has a resolution of 5.27 x 10^{-6} Oe, and at 10 Hz it is 9.33 x 10^{-6} Oe (Delooze et al, 2004). An improvement of the phase noise of the oscillator, electronics and the use of screening could further increase the performance of the sensor. With these improvements, the GMI sensor technique will be suitable for a wide range of bio-medical applications.

After 10pT resolution of GMI sensors was confirmed in a number of laboratories, GMI-wire and GMI-multilayers sensors were tested for use in the fields of advanced intelligent transport systems, public automation systems, and security systems. It further was recognised that GMI sensors may represent a viable alternative for the conventional biosensors. Firstly, GMI- wire sensors were used in magnetic immunoassays (Chiriac. & Herea, 2007). The sensor system contained a pair of glass-coated amorphous microwires one of them was copolymer-functionalized. The sensor response to the presence of different magnetic microparticles as perturbating agents for the external dc magnetic field was studied. This type of magnetic biosensor prototype was then used for biomolecule detection.

More importantly, the GMI sensor technology was applied for biological magnetic field detection. The GMI sensor based on C-MOS IC with a pair of amorphous wires for differential output was successfully applied for measurements of biocell magnetic fields (Mohri et al, 2009; Uchiyama et al, 2009). This kind of detection can be developed to become, for example, an organ prediction method for iPS cell growth. When compared with the microelectrode method of biocell measurement, the magnetic method benefits from non-invasion operations. The resolution of 10 pT was achieved when measuring the magnetic field generated by a smooth muscle tissue sample (4 mm width, 7 mm length, and 0.3 mm thickness) prepared from a guinea-pig bladder. The sample was dipped in an extracellular solution during the experiment. The pulsed wave was obtained due to Ca^{2+} flow through a membrane. The sample and differential sensor heads were separated by a cover glass. The distance from the sample to the upper sensor head was approximately 1mm. It is known that spontaneous electrical activities in smooth muscle cell clusters have a high temperature dependence (Nakayama et al, 2006). This was confirmed with magnetic detection. Maximum field strength of approximately 1 nT and a cyclic pulse wave can be observed at 33 degrees centigrade. Alternatively, the amplitude of the magnetic field is less than 50 pT and cyclic pulse wave cannot be observed at 27 degrees centigrade.

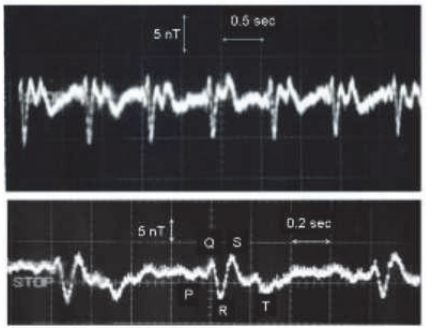

Fig. 19. Waveform of the cardiogram signal measured by CMOC GMI differential sensor in non-shielded environment.

Both GMI-wire and GMI multilayers sensors were used for detecting cardiac magnetic field. The long axis of the sensor head is aligned parallel to the chest surface. The cardiogram signal was clearly detected under the no shield environment when the sensor head is very close to the chest surface. The waveform of the cardiogram is shown in Fig. 19 obtained with GMI-wire sensor(Uchiyama et al, 2009). The features of QRS and T waves correspond with the electrocardiogram. The maximum field strength of several nT is almost 50 times larger than the magneto-cardiogram measurement by a SQUID system using Sensor-to-Chest spacing of approximately 50 mm (Fong et al; 2004).

7. Conclusions

This Chapter summarises some magnetic technology used for detecting and measuring magnetic fields from human subjects and from magnetically tagged bio substances. It develops the argument that there will be an increasing desire for more 'magnetic' information about the human body in the future. The desire for this information will need to further the development of modern magnetic sensor techniques to compete with the now

well-established SQUID magnetometer technology. Measuring and monitoring magnetic fields from the human body is becoming a rapidly increasing subject of research. The very expensive use of the SQUID magnetometer up until now has produced many advances in the understanding of magnetic fields from our bodies. The advance of much cheaper room-temperature sensor technologies offers the prospect of much greater use of magnetic field monitoring in medicine. In such cases it is also important to use low-cost shielding environments or carefully designed noise-suppressed detection systems. Two relatively new magnetic sensing technologies, namely, magnetoimpedance and magnetic particle spectroscopy, have a potential to replace the SQUID magnetometry in such areas as MCG and immunoassays.

8. References

Baibich, M.N.; Broto, J.M.; Fert, A.; Nguyen Van Dau, F.; Petroff, F.; Etiene, P; Creuzet, G.; Friederich, A.; Chazelas, J. (1988). Giant magnetoresistance of (001)Fe/(001)Cr magnetic superlattices. *Phys. Rev. Lett*. Vol. 61, No 21, November 1988, pp. 2472–2475.

Beach, R.S. & Berkowicz, A.E. (1994). Giant magnetic field dependent impedance of amorphous FeCoSiB wire. *Appl.Phys.Lett.*, Vol. 64, No. 26, Jun 1994, pp. 3652-3654, ISSN 0003-6951.

Chiriac, H. M. & Herea, D.D. (2007) Magneto-impedance sensor for biomedical applications. Journal of Applied Electromagnetics and Mechanics, Vol.25, No.1-4, pp. 453-459, ISSN: 1383-5416.

Chiriac, H. & Ovari, T.A. (1996). Amorphous glass-covered magnetic wires: preparation properties, applications. *Progress in Material Science*, Vol. 40, No. 5, February 1999, pp. 333-407, ISSN: 0079-6425.

D. De Cos, L. V. Panina, N. Fry, I. Orue, A. García-Arribas, and J. M. Barandiarán. (2005). Magnetoimpedance in narrow NiFe/Au/NiFe multilayer film systems. *IEEE Trans. Magn*. Vol. *41*, No 10, October 2005, pp. 3697-3699, ISSN 0018-9496.

Delooze, P.; Panina, L. V.; Mapps, D. J.; Ueno K.; Sano,H. (2004). Sub-nano tesla differential magnetic field sensor utilizing asymmetrical magneto impedance in multilayer films. *IEEE Trans. Magn*. Vol. *40*, No 4, pp. 2664-2666.

Delooze, P.; Panina, L. V.; Mapps, D. J.; Ueno K.; Sano,H. (2003). CoFeB/Cu layered film with crossed anisotropy for asymmetrical magneto-impedance. *IEEE Trans. Magn*. Vol. 39, No 5, pp. 3307-3309.

Fong, L.E.; Holzer, J.R.; McBride, K.K.; Lima, E.A.; Baudenbacher, F.; Radparvar, M. (2004) High-resolution imaging of cardiac biomagnetic fields using a low-transition temperature superconducting quantum interference device microscope, *Appl. Phys. Lett*., Vol. 84, pp. 3190-3192.

Garcia Prieto, M.J.; Pina, E.; Zhukov, A.P.; Larin, V.; Marin, P.; Vazquez, M., Hernando, A. (2000). Glass-coated Co-rich amorphous microwires with enhanced permeability. *Sensors and Actuators A: Physical*, Vol. 81, No. 1, April 2000, pp. 227-231, ISSN 0924-4247.

Gaster, R. S.; Hall, D. A.; Nielsen, C.H.; Osterfeld, S. J.; Yu, H.; Kathleen E. M., K. E.; Wilson, R. J.; Murmann, B.; Liao, J. C.; Gambhir, S. S.; Wang, S. X. (2009). Matrix-insensitive protein assays push the limits of biosensors in medicine. *Nature Medicine*, Vol. 15, No. 11, November 2009, pp. 1327-1333, ISSN 1078-8956.

Gleich, B. & Weizenecker, J. (2005) Tomographic imaging using the nonlinear response of magnetic particles. *Nature*, Vol. 435, 30 June 2005, pp. 1214-1217.

Graham, D.L.; Ferreira, H.A.; Freitas, P.P.(2004). Magnetoresistive-based biosensors and biochips. *Trends Biotechnol*. Vol. 22, No 9, September 2004, pp. 455–462.

Hall M. (2001). Low field measurements. U.K. Magnetics Society Conference on Magnetic Measurement Techniques and Applications, National Physical Laboratories, U.K., Wed 10th October 2001.

Haukanes, B.I.; Kvam, C. (1993) Application of magnetic beads in bioassays. *Nature Biotechnology*. Vol. 11, No 1, pp. 60–63.

Hika, K.; Panina, L.V.; Mohri, K. (1996). Magneto-Impedance in Sandwich Film for Magnetic Sensor Heads. *IEEE Trans Magn* , Vol. *32*, No. 5, pp. 4594-4596.

Honkura, Y. (2002) Development of amorphous wire type MI sensors for automobile use. *J. Magn. Magn. Mater*. Vol. 249, No. 1-2, August 2002, pp. 375-381, ISSN 0304-8853.

Iramina, K.; Kamei, H.; Yumoto, M.; Ueno S. (2001). Effects of repetition rate of electric stimulation on MEG and fMRI signals. *IEEE Trans. Mag*., Vol 37, No. 4, July 2001, pp. 2918-2920.

Iramina, K.; Yumoto, M.; Yoshikawa, K.; Kamei, H.; Ueno S. (1997) Measurement of Somatosensory evoked response using functional MR images and MEG. *IEEE Trans. Mag*. Vol. 33, No. 5, September 1997, pp. 4260-4262.

Knobel, K. & Pirota K. R. (2002) Giant magnetoimpedance: concepts and recent progress. *J Magn Magn Mater*, Vol. 242-245, Part 1, April 2002, pp. 33–40.

Larin, V. S.; Torcunov, A. V.; Zhukov, A. P.; Gonzalez, J.; Vazquez, M. & Panina, L. V. (2002). Preparation and properties of glass-coated microwires. *J. Magn. Magn. Mater*., Vol. 249, No.1-2, August 2002, pp. 39-45, ISSN 0304-8853.

Mahdi, H. & Mapps. D.J. (2000). High-T_c SQUIDS: the ultra sensitive sensors for non-destructive testing and biomagnetism. *European Journal of Sensors and Actuators*, Vol A81, No 1-3, April 2000, pp. 367-370.

Makhnovskiy, D.P.; Panina, L. V. & Mapps, D. J. (2001). Field-dependent surface impedance tensor in amorphous wires with two types of magnetic anisotropy: helical and circumferential, *Phys. Rev. B*, Vol. 63, No. 14, April 2001, pp. 144424-17, ISSN 1098-0121

Martinsa, V.C. ; Cardosoa, F.A.; Germanod, J.; Cardosoa, S.; Sousad, L.; Piedaded, M.; Freitas P.P.; Fonseca. L.P. (2009) Femtomolar limit of detection with a magnetoresistive biochip. *Biosensors and Bioelectronics*, Vol. 24, No. 8, pp. 2690–2695, ISSN 0956-5663.

Megens, M. & Prins, M. (2005). Magnetic biochips: a new option for sensitive diagnostics *J. Magn. Magn. Mater*. Vol. 293, No. 1, May 2005, pp. 702–708.

Mohri, K.; Humphrey, F.B.; Panina, L.V.; Honkura, Y.; Uchiyama, T.; Hirami, M. (2009). Advances of amorphous wire magnetics in 27 Years. *Phys. Stat. Solidi* A, Vol. 206, No. 4, April 2009, pp. 601-607.

Mohri K. & Honkura Y. (2007). Amorphous wire and CMOS IC based magneto-impedance sensors --- Orign, topics, and future. *Sensor Letters*, Vol. 5, No. 2, March 2007 pp. 267-270, ISSN 1546-198X.

Mohri, K.; Uchiyama, T.; Shen, L.P.; Cai, C.M.; Honkura, Y.; Aoyama, H.; (2002). Amorphous wire and CMOS IC-based sensitive micromagnetic sensors utilizing

magnetoimpedance (MI) and stress-impedance (SI) effects, *IEEE Trans Magn* Vol. **38**, pp. 3063–3068.

Mohri, K.; Uchiyama, T.; Shen, L.P.; Cai, C.M. & Panina, L.V. (2001). Sensitive micro magnetic sensor family utilizing magneto-impedance (MI) and stress-impedance (SI) effects for intelligent measurements and controls. *Sensors and Actuators, A: Physical*, Vol. 91 No. 1-2, June 2001, pp. 85-90, ISSN: 0924-4247

Morikawa, T.; Nishibe, Y.; Yamadera, H.; Nonomura, Y.; Takeuchi, M.; Taga, Y. (1997). Giant magneto-impedance effect in layered thin films. *IEEE Trans Magn* . Vol. *33* , No.5, September 1997, pp. 4367-4372, ISSN: 0018-9464.

Nakayama, S.; Shimono, K.; Liu, H.-N.; Jiko, H.; Katayama, N.; Tomita T., & Goto, K. (2006). Pacemaker phase shift in the absence of neural activity in guinea-pig stomach: a microelectrode array study, *J. Physiol.* Vol. 576, No. 3, pp. 727-738.

Nikitin, P.I. ; Vetoshko, P.M. ; Ksenevich, T.I. (2007) Magnetic Immunoassays. *Sensor Letters*, Vol. 5, No. 1, pp 296-298, ISSN 1546-198X.

Nikitin, P.I.; Vetoshko, P.M.; Ksenevich, T.I. (2007) New type of biosensor based on magnetic nanoparticle detection. *J. Magn. Magn. Mater*. Vol. 311, pp. 445-449.

Ogasawara, I. & Ueno, S. (1995). Preparation and properties of amorphous wires. *IEEE Trans. Magn*. Vol. *31,* No. 2, March 1995, pp. 1219-1223, ISSN 0018-9464.

Ong, K .G. & Grimes, C. A. (2002). Tracking the harmonic response of magnetically-soft sensors for wireless temperature, stress, and corrosive monitoring. *Sensors and Actuators A*, Vol. 101, pp. 49–61.

Panina, L.V. (2009). Magnetoimpedance (MI) in amorphous wires: new materials and applications. *Phys. Status Solidi A*, Vol.206, No.4, April 2009, pp. 656-662.

Panina, L. V.; Makhnovskiy, D. P.; Mohri, K. (2004) Magnetoimpedance in amorphous wires and multifunctional applications: from miniature magnetic sensors to tuneable microwave metamaterials, *JMMM*, Vol. 272, pp. 1452-1459.

Panina, L.V.; Zarechnuk, D.; D.P. Makhnovskiy, D. P.; Mapps, D.J. (2001). Two-dimensional analysis of magnetoimpedance in magnetic/metallic multi- layers. *J Appl Phys* , Vol. *89* , pp. 7221-7224.

Panina, L. V.; Makhnovskiy, D. P.; Mohri , K. (1999) Mechanism of asymmetrical magneto-impedance in amorphous wires. *J. Appl. Phys*, Vol. 85, pp. 5444-46.

Panina, L. V.; Mohri, K.; Bushida, K.; Noda, M. (1994). Giant Magneto-Impedance and Magneto-Inductive Effects in Amorphous Alloys. *J. Appl. Phys*, Vol. 76, pp 6198-6203.

Panina, L.V. & Mohri, K. (1994). Magneto-impedance effect in amorphous wires. Appl.Phys.Lett, Vol. 65, No. 9, August 1994, pp. 1189-1191, ISSN 0003-6951

Prinz, G.A. (1998) Magnetoelectronics. *Science,* Vol. 282, pp. 1660–1663.

Ripka, P. Magnetic sensors and magnetometers, Artech House Publishers (2001).

Phan, M. & Peng, H. (2008). Giant Magnetoimpedance Materials: Fundumentals and Applications. *Progress in Materials Science*, Vo.53, No 2, February 2008, pp 323-420.

Sandacci, S. I.; Makhnovskiy, D. P.; Panina, L. V.; Mohri, K. & Honkura, Y. (2004a) Off-diagonal impedance in amorphous wires and its application to linear magnetic sensors. *IEEE Trans Magn.*, Vol. 40, No. 6, November 2004, pp. 3505 – 3511, ISSN: 0018-9464.

Shen, L.P.; Uchiyama, T.; Mohri, K.; Kita, E. & Bushida, K. (1997). Sensitive stress-impedance micro sensor using amorphous magnetostrictive wire. *IEEE Transactions on Magnetics,* Vol. 33, No. 5, September1997, pp. 3355 – 3357, ISSN 0018-9464.

Sternickel, K. & Braginski A.I. (2006) Biomagnetism using SQUIDs: status and perspectives. Supercond. Sci. Technol. Vol. 19, No.3, pp. 3-6.

Takajo, M.; Yamasaki, J.; Humphrey, F.B.; (1993). Domain observations of Fe and Co based amorphous wires, IEEE Trans. Magn., Vol. 29, No 6, pp. 3484-3486, ISSN:0018-9464.

Tamanaha, C.R.; Mulvaney, S.P.; Rife, J.C.; Whitman, L.J. (2008). Magnetic labeling, detection, and system integration. *Biosens. Bioelectron*. Vol. 24, No. 1, September 2008, pp 1–13.

Ter Brake, H. J. M.; Wieringa H. J.; Rogalla, H. (1991). Improvement of the performance of a μ-metal magnetically shielded room by means of active compensation. Measurements Science & Technology. Vol. 2, No. 7, pp. 596-601, ISSN 0957-0233.

Uchiyama T.; Nakayama, S.; Mohri, K.; Bushida, K. (2009). Biomagnetic field detection using very high sensitive magneto-impedance sensors for medical applications. *Physica Status Solidi* (a). Vol. 206, No.4, april 2009, pp. 639-643.

Ueno, K.; Hiramoto, H.; Mohri, K.; Uchiyama, T.; Panina, L.V. (2000) Sensitive asymmetrical MI effect in crossed anisotropy sputtered films. *IEEE Trans. Magn*. Vol. *36*, No. 5, September 2000, pp. 3448-3450, ISSN 0018-9464

Vazquez, M.; Chiriac, H.; Zhukov, A; Panina, L. & Uchiyama T., On the state-of-the-art in magnetic microwires and expected trends for scientific and technological studies. *Phys. Status Solidi A*, Vol. 208, No. 3, March 2011, pp. 493–501 ISSN 1862-6300

Weizenecker, J; Gleich, B.; Rahmer, J.; Dahke, H.; Borgert, J. (2009) Three-dimensional real time in vivo magnetic particle imaging. *Phys. Med. Boil*., Vol. 54, pp. L1-L10.

Wikswo, J.P. (1999). Application of SQUID magnetometers to biomagnetism and nondestructive evaluation. Applications of Superconductivity, H. Weinstock, ed., Kluwer Academic Publications, 1999.

Wolf, S.A. *et al*.(2001) Spintronics: A spin-based electronics vision for the future. *Science,* Vol. 294, pp. 1488–1495.

Xu, L.; Yu, H.; Akhras, M.S.; Han, S.-J.; Osterfeld, S.; White, R.L.; Pourmand, N.; Wang, S.X. (2008) *Biosens. Bioelectron*. Vol. 24, pp. 99–103.

Yabukami, S.; Mawatari, H.; Murayama, Y.; Ozawa, T.; Ishiyama, K.; Arai, K.I. (2004). High-frequency carrier type thin-film sensor using low-noise crystal oscillator. *IEEE Trans. Magn.* Vol. 40, No. 4, July 2004, pp. 2670-2672, ISSN 0018-9464

Yabukami, S.; Suzuki, T.; Ajiro, N.; Kikuchi, H.; Yamaguchi, M.; Arai, K.I. A high frequency carrier-type magnetic field sensor using carrier suppressing circuit. *IEEE Trans. Magn.* Vol. 37, No. 4, July 2001, pp. 2019-2022, ISSN 0018-9464

Zhukov A. & Zhukova V. (2009). *Magnetic properties and applications of ferromagnetic microwires with amorphous and nanocrystalline structure*, Nova Science Publishers, ISBN: 978-1-60741-770-400, Hauppauge, NY, USA

Zhukov, A.; Ipatov, M.; Zhukova, V.; Garcia, C.; Gonzalez, J. & Blanco, J. M. (2008). Development of ultra-thin glass-coated amorphous microwires for HF magnetic sensor applications. *Phys. Stat. Sol. (A)*, Vol. 205, No. 6, June 2008, pp. 1367-1372, ISSN 1862-6300

Zhukov, A.; Gonzalez, J.; Blanco, J.M.; Vazquez, M. & Larin, V. (2000). Microwires coated by glass: A new family of soft and hard magnetic materials. *J. Mat. Res.*, Vol. 15, No. 10, October 2000, pp. 2107-2113, ISSN: 0884-2914

Zhukova, V; Ipatov, M. & Zhukov A., (2009) Thin Magnetically Soft Wires for Magnetic Microsensors. *Sensors* Vol. 9, No. 11, November 2009, pp. 9216-9240, ISSN 1424-8220

Zhukova, V.; Chizhik, A.; Zhukov, A.; Torcunov, A.; Larin, V. & Gonzalez, J. (2002), Optimization of giant magnetoimpedance in Co-rich amorphous microwires. *IEEE Trans. Magn.*, Vol. 38 No. 5, September2002, pp. 3090-3092, ISSN: 0018-9464

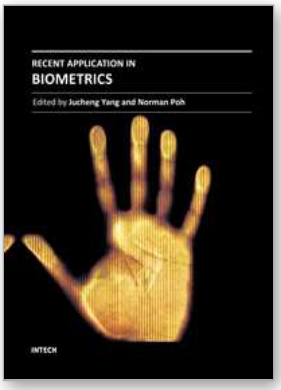

Recent Application in Biometrics

Edited by Dr. Jucheng Yang

ISBN 978-953-307-488-7
Hard cover, 302 pages
Publisher InTech
Published online 27, July, 2011
Published in print edition July, 2011

In the recent years, a number of recognition and authentication systems based on biometric measurements have been proposed. Algorithms and sensors have been developed to acquire and process many different biometric traits. Moreover, the biometric technology is being used in novel ways, with potential commercial and practical implications to our daily activities. The key objective of the book is to provide a collection of comprehensive references on some recent theoretical development as well as novel applications in biometrics. The topics covered in this book reflect well both aspects of development. They include biometric sample quality, privacy preserving and cancellable biometrics, contactless biometrics, novel and unconventional biometrics, and the technical challenges in implementing the technology in portable devices. The book consists of 15 chapters. It is divided into four sections, namely, biometric applications on mobile platforms, cancelable biometrics, biometric encryption, and other applications. The book was reviewed by editors Dr. Jucheng Yang and Dr. Norman Poh. We deeply appreciate the efforts of our guest editors: Dr. Girija Chetty, Dr. Loris Nanni, Dr. Jianjiang Feng, Dr. Dongsun Park and Dr. Sook Yoon, as well as a number of anonymous reviewers.

INTECH
open science | open minds

InTech Europe
University Campus STeP Ri
Slavka Krautzeka 83/A
51000 Rijeka, Croatia
Phone: +385 (51) 770 447
Fax: +385 (51) 686 166
www.intechopen.com

InTech China
Unit 405, Office Block, Hotel Equatorial Shanghai
No.65, Yan An Road (West), Shanghai, 200040, China
中国上海市延安西路65号上海国际贵都大饭店办公楼405单元
Phone: +86-21-62489820
Fax: +86-21-62489821